EDUCACIÓN
SECRETARÍA DE EDUCACIÓN PÚBLICA

Instituto Politécnico Nacional
"La Técnica al Servicio de la Patria"

Research in Computing Science

Vol. 155 No. 2
February 2026

Research in Computing Science

Research in Computing Science, Año 25, Volumen 155, No. 2, febrero de 2026, es una publicación mensual, editada por el Instituto Politécnico Nacional, a través del Centro de Investigación en Computación. Av. Juan de Dios Bátiz S/N, Esq. Av. Miguel Othon de Mendizábal, Col. Nueva Industrial Vallejo, C.P. 07738, Ciudad de México, Tel. 57 29 60 00, ext. 56571. https://www.rcs.cic.ipn.mx. Editor responsable: Dr. Grigori Sidorov. Reserva de Derechos al Uso Exclusivo del Título No. 04-2019-082310242100-203. ISSN: en trámite, ambos otorgados por el Instituto Politécnico Nacional de Derecho de Autor. Responsable de la última actualización de este número: el Centro de Investigación en Computación, Dr. Grigori Sidorov, Av. Juan de Dios Bátiz S/N, Esq. Av. Miguel Othon de Mendizábal, Col. Nueva Industrial Vallejo, C.P. 07738. Fecha de última modificación 01 de febrero de 2026.

Research in Computing Science, year 25, Volume 155, No. 2, February 2026, is published monthly by the Center for Computing Research of IPN.

Volume 155(2)

Advances in Computing Science

Alexander Gelbukh (ed.)

Instituto Politécnico Nacional, Centro de Investigación en Computación
México 2026

ISSN: in process

Formerly ISSNs: 1870-4069, 1665-9899

Instituto Politécnico Nacional (IPN)
Centro de Investigación en Computación (CIC)
Av. Juan de Dios Bátiz s/n esq. M. Othón de Mendizábal
Unidad Profesional "Adolfo López Mateos", Zacatenco
07738, México D.F., México

http://www.rcs.cic.ipn.mx
http://www.ipn.mx
http://www.cic.ipn.mx

Indexed in LATINDEX, DBLP and Periodica

Electronic edition

ISSN 1870-4069

Table of Contents

ISSN 1870-4069

Comparison of Parsing Techniques

Nida Hafeez[1,2], Muhammad Ateeb Ather[2], Abdollah Abadian[1], José Luis Oropeza Rodríguez[1]

[1] Instituto Politécnico Nacional (IPN), Centro de Investigación en Computación (CIC), Mexico City, Mexico

[2] Bahria University, Lahore, Department of Computer Sciences, Pakistan

03-134211-022@student.bahria.edu.pk

Abstract: This review paper provides a thorough examination of compiler building parsing methods. It emphasized the significance of parsing in compiler construction and the requirement for effective and precise parsing algorithms. The paper examines a number of parsing strategies, including top-down and bottom-up parsing, discussing both traditional approaches and more contemporary developments. The evaluation considers variables including time complexity, error recovery, support for ambiguous grammar, and simplicity of implementation. Additionally, the effects of grammar traits and problem-solving techniques are covered. In order to increase the effectiveness and dependability of compiler construction, this paper offers researchers and practitioners useful insights and recommendations for selecting and implementing parsing strategies in compiler projects.

Keywords: Parsing, top-down, bottom-up, semantics, syntax, compiler, predictive parsing.

1 Introduction

Compiler converts a high-level language program to a low-level language program which a computer can understand and interpret. To achieve this conversion, the compiler passes the program through various phases. Each one of these phases has a unique role to play during the conversion. One of them is Parsing. Parsing in simple English language means to break down the sentence into grammatical parts and then identifying those parts and their relation to one another just like that, Parsing in Compiler Construction is breaking down the program into the grammatical rules of the high language to identify the syntax of the program.

Parsing is done in order to generate the syntax of the targeted grammar and then the syntax can also be verified using the same technique. Parsing is done by a part of the compiler named Parser. According to Hassan. Et. Al [2]. The main aim of parsing is to determine whether the string is part of the grammar or not. This can be achieved through various parsing techniques.

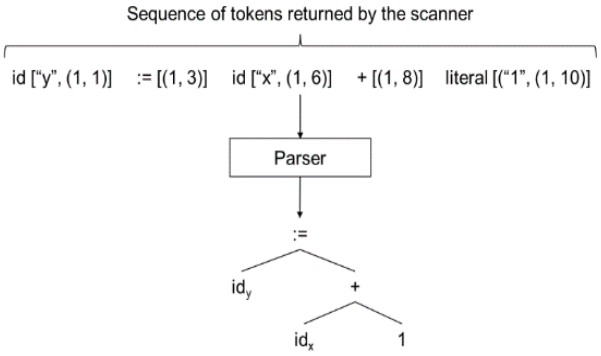

Fig. 1 Sequence of tokens returned by the scanner.

Out of all the parsing techniques two which are most widely used and discussed are top- down parsing and bottom-up parsing, based on these approaches the parser designed are either top-down parsers or bottom-up. Both the techniques are different depending on their names, the top-down parsing starts tracking down from the start of the production to the bottom whereas the bottom-up technique winds up the tracking from the end of the production to the start. Different techniques of parsing having their own pros and cons are not only used in compiler construction but are widely used in other fields of computer sciences such as Natural Language Processing (NLP), Robotics, Machine Learning(ML), Databases and even in Web Development. Due to the importance of parsing in multiple domains of Computer Science it is one of the most researched topics of Compiler Construction.

2 Literature Review

A. Parser

The role of the parser is to verify the syntax of the language used. The main function of the parser is to take in the final output from the lexical analyzer and then it uses the parsing techniques to verify the syntax. If the program is not syntactically correct, then the parser throws out the syntax error and if the syntax is verified then it generates the parsing tree of the CFG. The parser must have an error detection mechanism to detect errors in the syntax.

There are two approaches to define the grammars:

i. Context-Free Grammar,

ii. Parsing Expression grammar.

Parsing Expression grammar or PEG is a formal grammar to define formal languages using a set of rules to recognize that the string belongs to the language. PEG has only one valid abstract syntax tree for each grammar. This makes sure that the grammar is not ambiguous [4].

The work of the parser can be visualized.

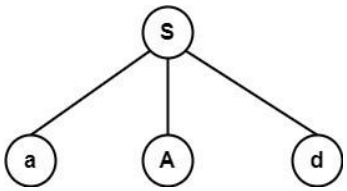

Fig. 2(a) shows the first production i.e., a Ad.

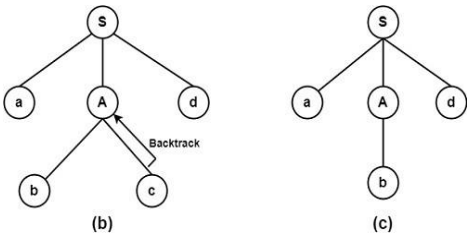

Fig. 2(b) shows that the production A → b c.

B. Top-Down Parsing

Top- down parsing is the parsing technique in which the parser starts to match the statement from the top of the parse tree and tries to match with the rules of the grammar. Top-down parsing involves the left derivation of the tokens and utilizes the expansion of terminal symbols. Backtracking is vital to have optimal solution using the top-down parsing.

Following are the types of top-down parsing techniques:

a. Backtracking

Backtracking is a technique in which the alternatives are used to expand the non-terminals. If one alternative does not work the other one is adopted. The mechanism is that if the opted set of rules does not verify the syntax, then the analyzer restarts, this time with a different set of rules which weren't used before. Consider the following grammar:

Input: S → aAd

A → bc | b

"abd" is the required string and "abcd" is not required.

It is used and the string abcd is formed, which is not a required string so it backtracks. Fig.2(b) shows that the alternative production which is A → b is used to obtain the required string "abd".

Backtracking is easier to implement. To backtrack to the previous state the backtracking technique keeps the states saved. The code is also small in size. Solving the large problem with backtracking is not effective as the technique becomes quite slow for the large problems and also it requires so much space to store all the states to backtrack the alternative rules. Due to the investigation of several paths, backtracking parsers may behave in a non- deterministic manner. As a result, the parsing outcomes could be less predictable. The chosen alternative might rely on how the options are explored or on other variables. Error reporting and recovery may become more difficult as a result. Due to all these reasons parsing techniques without backtracking are preferred.

b. Predictive Parsing

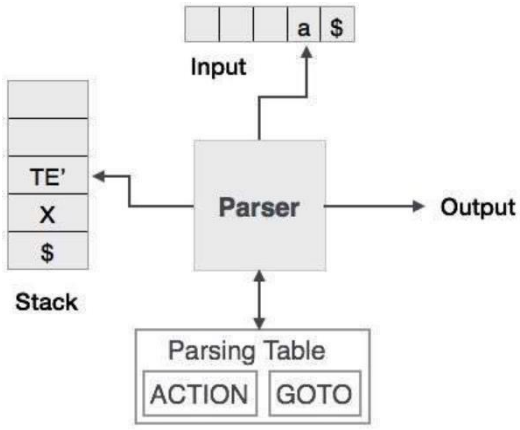

Fig. 3. Shows the predictive parsing components.

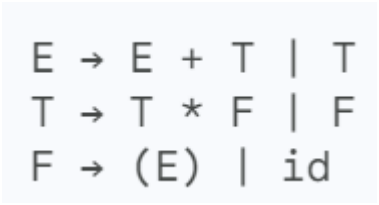

Fig. 4. (a) shows the grammar which can be used in predictive parsing

Fig. 4. (b) shows grammar which cannot be used in predictive parsing.

Predictive parsing is recursive descent parsing with the aim of predicting which of the productions is best to substitute the input string. Parse tree is constructed from the topmost symbol, input string is read from leftward side towards right side. This technique iteratively construes the input string and then the parsing tree is generated [5].

Predictive parsing has a stack to store the production symbols in the stack, whereas the input contains the input string that has to be verified. The third thing that the table contains is the production. If the top of the stack and the top of the input stack are the same, then we pop it out from both stacks and this way if both stacks have $ sign left then the string is verified and if input stack contain one or more than one such symbol which cannot be popped when compared with the stack then the string cannot be verified using the grammar.

Predictive parsing does not need backtracking and thus it uses only grammar which are backtrackless. To achieve this, the left recursion and the left factoring has to be removed from the grammar, basically making it backtrackless, which makes the process extensive. The only grammar that predictive parsing can use is LL(k) grammar where there is no ambiguity and left recursion.

Predictive parsing is a strong tool and provides flexibility to try out other alternatives but the fact that it cannot use all the grammar makes it to be used in certain cases only.

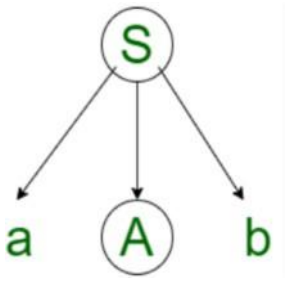

Fig. 5. (a) shows that the first production is used to start the parse tree.

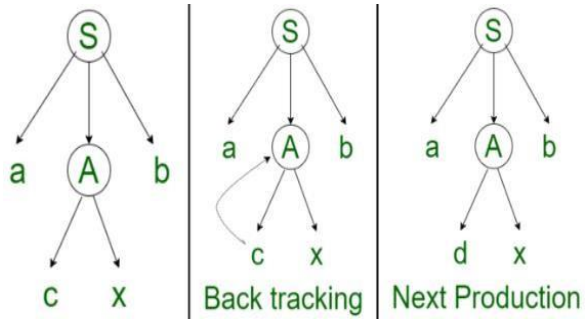

Fig. 5. (b) shows that the next production.

c. Recursive Descent Parsing

Recursive descent parsing is the type of parsing in which the parser is implemented using a set of recursive procedures, each corresponding to the non-terminal of the grammar. The parser starts with the top-level non-terminal and recursively invokes the corresponding procedures to parse the input string, making decisions based on the current input symbol.

Predictive parsing can also be called a special type of recursive descent parsing in which the backtracking is not possible. But both techniques have few differences such as the predictive parsing use of the first and follow sets, also the table is required to parse and predict which of the next production has to be used.

The recursive descent can or cannot use backtracking depending on what kind of grammar is being used to parse, whereas backtracking is not possible in predictive parsing. The recursive descent parsing use the left most input symbol to recursively analyze and then the parse tree is generated [5].

For instance:

Input string:

adxb S → aAb|aBb

A → cx | dx

B → xe

A → cx is used but this production does not verify the production so in Fig.5(c) shows that the backtracking is done and in Fig.5(d) the next production i.e. A → dx is used which verify the input string.

By using this technique, we cannot use objects other than global semantics, as recursion is to be done so the previous state has to be stored which requires memory.

	First	Follow
S –> A/a	{ a }	{ $ }
A –>a	{ a }	{ $ }

Fig. 6. (a) shows the first and follow set of the above grammar.

	a	$
S	S –> A, S –> a	
A	A –> a	

Fig. 6. (b) shows the table for the LL parsing.

d. LL Parsing

LL parsing is the left-left parsing, in which the first left defines that the input will be scanned from left to the right and the second left shows that the left derivation is used for parsing trees.

In this parsing first the first and follow sets of the productions are formed and after that the table is formed in which the rows are composed of non-terminals whereas the columns are made up of terminals. Any cell with no entry corresponds to different firsts and follow sets. If any cell contains more than one production that means that the grammar is ambiguous, and the LL parsing can't be done on that ambiguous grammar [3].

Consider the following grammar:

$$S \rightarrow A \mid a \; A \rightarrow a$$

As one of the cells contains two production rules that means the grammar is ambiguous and the LL parsing of this grammar is not possible until and unless the ambiguity is removed

LL parsing is also known as LL(k) parsing if it uses K tokens of look-ahead when parsing a sentence. Looking ahead at the next symbol helps in deciding which choice to make. The top-down parser does the prediction of input, and this prediction has a terminal symbol in front [6].

e. Bottom-up Parsing

As the name suggests, bottom-up parsing is a parsing technique in which the grammar productions are used in the opposite way, i.e., starting from the right and working its way up to the starting symbol. Due to the bottom to top approach used in this parsing it is known as bottom-up parsing. It is commonly used in the implementation of compilers and language processors. Bottom-up parsing uses a stack- based approach to identify and reduce groups of terminals and non-terminals until the input string is fully parsed.

It contains the following:

- Stack (to store),
- Output (provide results),
- Input (given to parser),
- Driver program (Same for all LR Parsers),
- Parsing Table (has two functions “Action”, “Go To”, varies from parser to parser).

Bottom-up parsing is often based on the shift- reduce parsing strategy. The parser scans the input string from left to right, shifting terminals onto a stack until it can reduce a production rule and replaces them with the corresponding non- terminal.

The bottom-up parser maintains a stack to store the symbols encountered during the parsing process. It also maintains an input buffer containing the remaining input symbols that are yet to be parsed. Group of symbols on the stack to a non-terminal using a production rule [10].

It is required to have a handle recognizer which will assist in deciding appropriate action, by perusing the stack. FSM (finite-state-machine) operates as a recognizer. Nevertheless, here terminals and non-terminals are included in language symbols. Last state or final state indicates success or reduction by dropping it out, when following any rules [5].

There are two basic actions in Bottom-up- parsing:

- Move present input token in stack also, read next token.
- Reduce by rule of production.

Bottom-up parsing is powerful and can handle a wide range of context-free grammar, including ambiguous and left-recursive grammar. It provides greater expressiveness and flexibility compared to some other parsing techniques. Bottom-up parsers are generally better at error recovery compared to top-down parsers. They can often continue parsing after an error and recover to a valid state, reducing the impact of syntax errors on the overall parsing process.

f. Precedence Parsing

Precedence parsing is a technique for code analysis that employs operator precedence to resolve conflicts between many potential code meanings. Because the order of operations and the associativity of operators must be considered when parsing expressions and arithmetic operations, it is especially helpful in these situations.

There are two type of precedence parsing:

a) Operator Precedence

Operator Precedence Parsing is a method of precedence parsing that utilizes an operator precedence table. The table specifies the precedence and associativity of operators in the grammar. It is constructed based on the grammar's production rules and the operators used.

b) Simple Precedence

Simple Precedence Parsing is another type of precedence parsing that uses a simple precedence relation between adjacent non- terminals. It is a more relaxed version of Operator Precedence Parsing and can handle a wider range of grammars.

g. LR Parsing

LR parsing is the most commonly known bottom-up parsing technique used in compiler construction to construct the tree. It generally stands for Left Right derivation, it is of different types like LALR, SLR etc. [11].

1. SLR

SLR stands for simple Left Right derivation and it's the most simple and efficient one from the rest of the LR parsing techniques. It is based on LR(0) and uses a simplified LR parsing table. It is widely used in compiler construction because it's easier to implement yet a reasonably powerful technique [9].

2. LALR

Look-ahead ahead LR is the parsing technique that has a look-ahead pointer and is used to create a compact yet efficient compiler for context-free grammar. LALR is the extension of SLR, addressing the limitations of the SLR by increasing the power of the parsing yet keeping it quite efficient [8]. LALR can resolve more shift-reduce and reduce-reduce conflicts, making it much more powerful than SLR. LALR basically uses a small parsing table, therefore decreasing the need for the memory needed to store the states of the table. But still

LALR is not as powerful as the expressive LR(1) parsing technique.

3. GLR

It is used commonly for the following reasons:

1. Great parsing efficiency.

2. Effective error recovery [7].

GLR has active support for recovery against error. The foremost contributions are

1. GLR provides fast parsing speed with LALR (1).

2. Additional fault retrieval mechanisms [3].

4. CYK (Cocke-Younger-Kasami)

CYK is not appropriate as it has large time space complexity. It does not have a static direction of scanning and a complete source is essential to be read as an early step while parsing. It means, it cannot be utilized in parsing huge legacy-systems. Ideal algorithm must be able to:

- Parse any given context-free grammar.

Table 1. Shows the comparison of Parsing Technique and their applicability.

Technique	Advantage	Limitation	Applicability
Recursive Descent Parsing	Easy to implement and understand, suitable for LL(k) grammars	Inefficient for left-recursive grammars, struggles with ambiguity	Simple grammars, LL(k) grammars
LL(k)	Efficient for LL(k) grammars, top-down parsing, good error reporting	Limited support for left- recursive grammars, k-factor lookahead restriction	LL(k) grammars, non- left-recursive grammars
LR(k)	Efficient for LR(k) grammars, handles left-recursion, broad language coverage	Complex implementation, potentially ambiguous grammars require resolution	LR(k) grammars, general-purpose parsing
LALR(1)	Efficient, compact parsing tables, broader language coverage than LL(k)	Efficient, compact parsing tables, broader language coverage than LL(k)	LR(0) grammars, practical applications
GLR	Handles ambiguous grammars, multiple parse tree generation, broad language coverage	Increased memory usage, potentially slower due to ambiguity resolution	Ambiguous grammars, natural language processing
Packrat	Linear time parsing for grammars with limited backtracking, good error reporting	Increased memory usage, not suitable for all grammars	Parsing with limited backtracking, PEG grammars

- Image input from left to right.
- Eliminate backtracking.
- GLR rightly fulfills these requirements [2].

5. Recursive Ascent Parser

a. Packrat parser

It provides flexibility as well as ability of backtracking and unrestricted lookahead, but nevertheless guarantees linear parse time [5]. It does not require any special lexical analyzer.

3 Differences

Two popular methods for creating parsers are top-down and bottom-up parsing. While bottom-up parsing starts with the input and groups terminals into non-terminals, top-down parsing starts with the root and extends non- terminals to match the input string.

Top-down parsing offers clearer error signals and is more practical for simpler grammar. Bottom-up parsing, on the other hand, is more potent, effective for bigger grammar, and better at error recovery.

The complexity and requirements of the grammar determine which of the two approaches is best.

In contrast to bottom-up parsing, which is better for complex grammars with left-recursion, ambiguity, or LR(k) features, top-down parsing is recommended for less complicated, unambiguous, and LL(k) grammars.

The final choice ought to be dependent on the particular grammar and parsing requirements.

4 Future Work

Future work on this article includes investigating novel parsing techniques, improving performance through sophisticated algorithms and parallel processing, creating reliable error recovery and correction methods, handling complex grammars with specialized techniques, integrating parsing with other compiler phases, and performing empirical studies on real-world applications. These research directions seek to deepen our comprehension of parsing methods, better compiler performance generally, and facilitate the creation of more dependable and efficient compilers for a variety of programming languages and applications.

5 Conclusion

In conclusion, the different kinds of parsers used in real-time applications have been discussed in this study. We have reviewed a number of parsing algorithms; in terms of comparison, bottom-up approaches are the most effective but difficult to implement; backtracking is not required, but handling is implemented. However, top-down parsing

is straightforward whereas backtracking is occasionally necessary, where both parsing methods are appropriate, backtracking can be removed using predictive parsing, making top-down parsing simple to use.

References

1. Angelo Borsotti, L. B.: General parsing with regular expression matching. Journal of Computer Languages, 74, (2022). doi:10.1016/j.cola.2022.10 1176.
2. Hamna Baqai, A. I. Comparison of Parsing Techniques (2020)
3. Hassan Ali, M. S.: LL(1) (2020)
4. Parser versus GNF inducted LL(1) Parser on Arithmetic Expressions. Quest research journal (2010)
5. Hnin Myat Soe, D. M.: Implementation of Learning for Syntax Analyzer. *Fourth* Local Conference on Parallel and Soft Computing (2009)
6. Ismail A. Ismail, N. A.: Internet of things -application and future. 114, pp. 115–124 (2019)
7. Moore, J.: Introduction to Compiler Design. pp. 14–32 (2019)
8. van Binsbergen, L.T.: Purely functional GLL parsing. Journal of Computer Languages, 58, (2020). doi:10.1016/j.cola.2020.10 0945.
9. Oudshoorn, M.: A Drop-in Replacement for LR[1] Table-Driven Parsing. Journal of Advances in Computing and Engineering, 1(2) (2021)
10. Pankaj Sharma, N. M. Parsing Techniques: A Review. International Journal of Advanced Research in, 2(10) (2019)
11. Wyk, E. V.: Context in Parsing: Techniques and Application (2023). doi:10.4230/OASIcs.EVCS.2023.18.
12. Zimmerman, J.: Practical LR Parser Generation. Formal Languages and Automata theory (2022)

ISSN 1870-4069

Corneal Topography Using a Null-screen Target in a Quadrangular Prism Configuration

M. I. Rodríguez-Rodríguez[1,*], A. Abril Suarez-Ajoleza[1],
D. Aguirre-Aguirre[2], D. González-Utrera[2],
R. Díaz-Uribe[2], A. Carmichael Martins[3], Brian Vohnsen[4]

[1] Facultad de Estudios Superiores Iztacala UNAM,
Mexico

[2] Instituto de Ciencias Aplicadas y Tecnología,
Universidad Nacional Autónoma de México,
Mexico

[3] Indiana University School of Optometry, Bloomington,
Ireland

[4]Advanced Optical Imaging Group, School of Physics,
University College Dublin,
Ireland

martin.isaias.rodriguez@iztacala.unam.mx

Abstract. In previous works, three reflective calibration spheres of different radius of curvature (7.7 mm, 9.42 mm, and 6.20 mm) were evaluated using an experimental setup based on specular reflection. To build this system; we use four identical null-screens into a quadrangular acrylic prism. The aim of this work is to show that the same setup is suitable as a corneal topographer instead of the traditional commercial topographers based in Placido disk. To achieve this purpose, experimental images of a volunteer´s cornea were obtained from the reflection of an adaptable Hartmann-pattern. With the experimental parameters of the elements involved in the setup and the spot centroid data obtained by image processing, the local normals of the surface at sampled points were found. Accurate reconstruction of the surface shape of a human cornea is obtained by numerical integration of the normals. By fitting the recovered data to a spherical model the corresponding elevation map and radius of curvature 7.84 mm were found. This is the first report of the evaluation of a corneal surface using a null-screen target in a quadrangular prism configuration.

Keywords: Null-Screens, Hartmann pattern, numeric integration method, corneal topography.

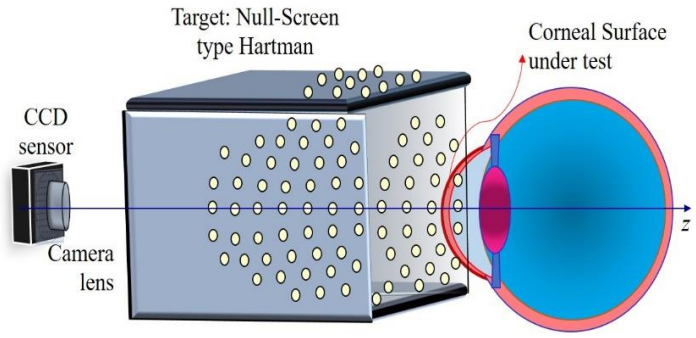

Fig. 1. Schematic setup of a quadrangular prism configuration [10].

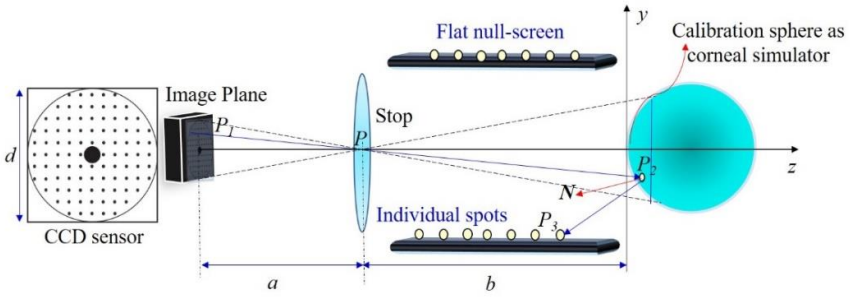

Fig. 2. Variables involved in the calculation of flat null-screen.

1. Introduction

It is well known that the anterior corneal surface provides about three-quarters parts of the total dioptric power of the human eye. On the other hand, refractive corrections and monitoring of corneal ectasias and keratoconus are all measured by corneal topography. Thus, quantifying corneal parameters such as radius of curvature, refractive power and elevation maps are of great research value and essential for vision and diagnostics. The studies about corneal topography have typically made use of a Placido disc or Scheimpflug ophthalmology [1]. However, a possible limitation of Placido system due to data ambiguity in azimuthal direction was reported in 1998 by Schwiegerling et al. [2], what's more; "Axial curvature and the skew ray error in corneal topography" was reported in 1997 by S.A. Klein [3-4]. Consequently, new generations of topographers were developed making use of different principles with a geometrical pattern of spots printed on null-screens and in a modified Hartmann test to measure corneal topography [5-7]. These recent advances have been successful in testing, because modifying the geometry it can overcome the skew ray error.

The null-screen method has been used to test different types of optical surfaces as; spherical, aspherical fast convex and recently freeform surfaces [5-9]. For this reason,

we have been working on a method for testing the corneal surface with four flat null-screens in a quadrangular prism setup, based on the null-screen principles. In a previous work, we have demonstrated quantitatively that three reflective calibration spheres of different radius of curvature; 7.7 mm, 9.42 mm, and 6.20 mm can be evaluated using the same experimental setup based on specular reflection [10]. This work aims to show that the same setup is suitable as a corneal topographer.

In Section 2, the proposed method is briefly described; then, the design parameters of the null-screen are shown and the experimental setup is fully explained in Sections 3 and 4, respectively. Later, in Section 5, experimental results of the corneal surface reconstruction of a human volunteer are presented. Finally, the conclusions are presented in Section 6.

2. Proposed Setup and Method

As mentioned before, we use four identical null-screens type Hartmann into a quadrangular acrylic prism. The corneal surface of a human volunteer is placed just in front of the quadrangular prism, as shown in Fig. 1.

The essential idea consists of designing an array of null screens with a set of spots in such a way that the image reflected by the corneal surface gives a perfectly ordered arrangement type Hartmann, if the test surface is perfect. Null-screen testing has the advantage that this technique does not need any additional optical element with a specific design to correct the aberrations of the system under test and the spots of the screen can be easily computed [8].

3. Parameters to the Design of Flat Null-Screen

To determine the points on the null-screen belonging to a square array of spots on the CCD sensor, we performed a reverse exact ray-tracing calculation, similarly as they have been obtained in previous work [6]; we use the same expression to get z_3, the calculation only differs in the use of four flat null-screens (parallel to the x and y axes), instead of three. In null-screen method is used to find the coordinates of the points on screen $P_3=(x_3, y_3, z_3)$ that yield a perfect square array on the CCD; then, we start at the CCD plane. The variables involved in the design of the flat null-screen are shown in Fig. 2; in addition, a calibration sphere is placed as a corneal simulator.

The point $P_1=(x_1, y_1,-a-b)$ and the point $P_2=(x_2, y_2, z_2)$ are the cartesian coordinates on the CCD sensor and in the optical surface respectively, *a* and *b* are distances obtained by the *Gauss thin lens equation* and by the *magnification of the lens used*, these equations can be seen in detail in ref. [6]. The parameters *a* and *b* can be recalculated using the proposal developed by Aguirre-Aguirre et al, ref. [11]. The numerical values of the parameters used in this case are shown in Table 1.

Table 1. Parameters used for calculating the coordinates of flat null-screens.

Element	Description	Symbol	Value (*mm*)
CCD sensor	Thorlabs Model (**DCU223M**)	*d*	3.6 active area
Camera lens	Thorlabs Model (**MVL25M23**)	*f*	25
Parameter	Distance between CCD sensor and camera lens	*a*	29.61
Parameter	Distance between vertex surface and camera lens	*b*	266.07

4. Experimental Setup

To build the practical system, we used four identical flat screens, their dimensions are: 260 mm (height) × 180 mm (width) per side correspondingly. The screens were put side by side to form a quadrangular prism. To classify each null-screen-colored marking (R, G, B and Y) have been designed, which, help to distinguish each side of null-screens inserted in the rectangular prism. As a proof of this principle, Fig. 3. (a) shows a low-cost experimental setup based on specular reflection. The image of the light reflected by the human cornea is nearly seen as a square array of dots captured by the CCD sensor, as is shown in Fig. 3. (b). The reflection of the adaptable Hartmann pattern provides data allowing accurate reconstruction of the surface profile of the corneal surface.

It can be seen that at some points of the null-screen, we paint strategic marks of color following the next basic rules: Six colored spots are set along the *x*-axis, while six spots are positioned along the *y*-axis. For example in Fig. 3 (a), we can see six red spots in the experimental setup along the *z*-axis, just to be redundant, in the orthogonal side, it is easy to see six green spots along the *z*-axis. This set of colored spots allows relating "*x*" and "*y*" directions on the screens even if one-or two-colored spots are missing. Due to the sticking of null-screens on edges of the square prism some spots on the image are missing; that, complicates the final correspondence between centroids and coordinates of the null-screens. For this, the same reference color marks designed in null-screens (R, G, B and Y) helps to the correspondence during the quantitative evaluation of optical surfaces [Fig. 3. (b)].

4.1 Zonal Integration

Having the information of the positions of the centroids and the knowledge coordinate to the flat null-screens, normal components to the surface are calculated, according to procedures proposed in [5-6], [9-11]. To evaluate the normals ***N***, to the test surface, we perform a three-dimensional ray trace procedure, which consists of finding directions of the rays that join actual positions, P_1, of centroids of the experimental image, and the

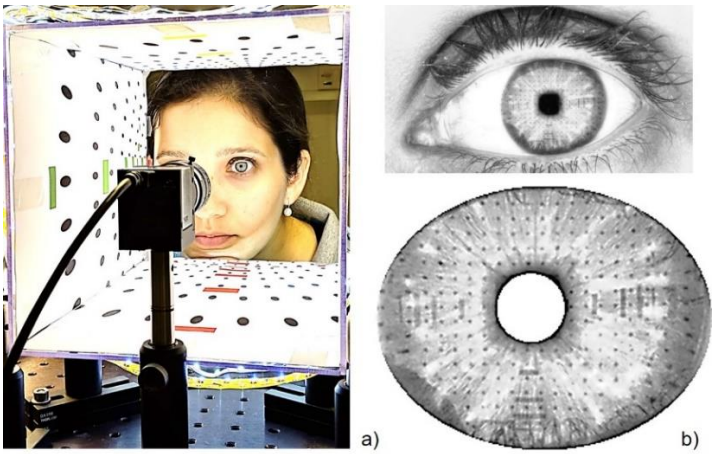

Fig. 3. (a) Experimental setup of corneal Topographer, (b) Detail of the reflected pattern.

corresponding coordinates *P3* of null-screen. According to reflection law, normal ***N*** to the test surface can be evaluated as.

$$N = \frac{R - I}{|R - I|}. \tag{1}$$

Where ***I*** and ***R*** are the directions of the incident and reflected rays on the surface, respectively. The direction of the reflected ray ***R*** is known because after reflection on the test surface it passes through the center of the lens stop at ***P*** and arrives at the CCD image plane at $\boldsymbol{P_1}$, so that, we have two points along this ray, which are enough to know its direction (see Fig. 2). In contrast, for incident ray ***I***, we know only the point $\boldsymbol{P_3}$ at null-screen, so, we need to have an approximate second point to obtain the direction of the incident ray; this is done by intersecting the reflected ray with a *reference surface*.

The shape of the surface is obtained by using the equation originally proposed by Díaz-Uribe [12] and first used in [8].

$$z - z_1 = \int_{\wp(x_1, y_1)}^{(x,y)} \left[\frac{N_x}{N_z} dx + \frac{N_y}{N_z} dy \right]. \tag{2}$$

Where; $\boldsymbol{N}x$, $\boldsymbol{N}y$, and $\boldsymbol{N}_z$ are the cartesian components of the normal vector, C is the integration path, z_1 is the initial point in the integration path. Eq. (2) is exact, evaluating normals and performing the numerical integration, however, are approximate, so they introduce some errors that must be reduced. Thus, the errors involved during the determination of the normals are minimal if the reference surface differs only slightly from the test surface. The numerical evaluation of Eq. (3) can be performed by zonal or modal procedures; a simple zonal evaluation of the integral is the trapezoidal rule for nonequally spaced data [12-13], as

Table 2. Principal Coefficients of the Zernike Standard Polynomial.

Zernike Standard Polynomial	Coefficient (**μm**)	Zernike Standard Polynomial	Coefficient (**μm**)
Vertical Astigmatism (Z_6)	14.0357	Vertical Coma (Z_7)	5.4472
Primary Spherical (Z_{11})	7.4266	Horizontal Coma (Z_8)	-3.2004

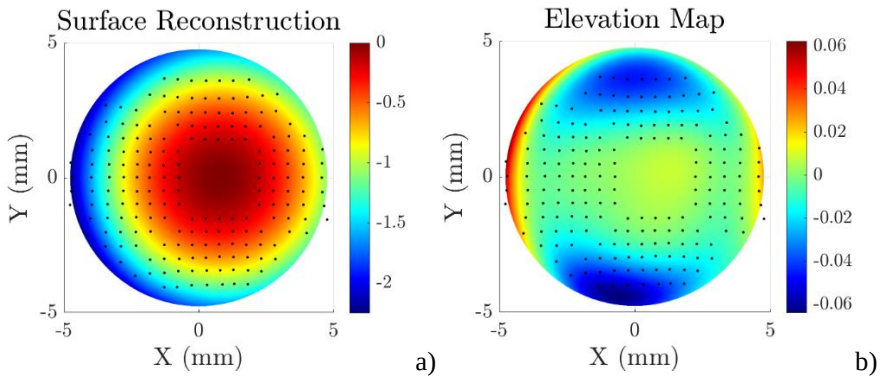

Fig. 4. Results: a) Shape surface reconstruction obtained by Zonal integration method, b) Elevation Color Map represented by Zernike standard Polynomial, (in mm units).

$$z_M = -\sum_{i=1}^{M-1}\left\{\left(\frac{N_{x_i}}{N_{z_i}}+\frac{N_{x_{i+1}}}{N_{z_{i+1}}}\right)\left(\frac{x_{i+1}-x_i}{2}\right)+\left(\frac{N_{y_i}}{N_{z_i}}+\frac{N_{y_{i+1}}}{N_{z_{i+1}}}\right)\left(\frac{y_{i+1}-y_i}{2}\right)+z_0\right\}. \quad (3)$$

Where M is the number of points along some integration path.
Consequently, the integration obtained with Eq. (3) and different paths covering all the centroids, the spatial position of every incidence point on the surface is obtained, and the shape surface equation is calculated as described in Refs. [5, 6].

5. Experimental Results

Corneal surface reconstruction obtained by the zonal integration method is shown in Fig 4(a). In addition, we obtained the elevation map (Fig. 4(b)) by taking the differences between the best spherical model and the data obtained by zonal integration. The differences were fitted into a Zernike standard polynomial with 37 terms [14].

In this first evaluation, we found that the radius of curvature of the best fitted sphere was $r_c = 7.84\ mm$. Analyzing the elevation color map, the peak-valley (P–V) value in sagitta differences is $\delta z_{p-v} = 120\mu m$, while the *RMS* value is $\delta z_{rms} = 18\ \mu m$. Table 2 lists the dominating Zernike components from the best fitted sphere. Results show that the dominated component is vertical astigmatism (Z_6).

6. Conclusions

In this paper, a quadrangular prism configuration based on null-screens has been proposed. This aimed at the measurement of corneal topography, so experimental results obtained for a human corneal have been presented. The radius of curvature becomes closer to the real value; on the other hand, the RMS difference in sagitta which represent the elevation color map is within the range of commercial topographers, with $\delta z_{RMS} = 18\ mm$. Finally, we notice that the dominating components of the Zernike standard polynomials are Astigmatism (Z_6, Z_8), Primary Spherical (Z_{11}), Vertical Coma (Z_7) and Horizontal Coma (Z_8). The results obtained do not represent a fundamental limit; they can be improved with better alignment of the quadrangular setup of the surface or by improving the numerical routines.

Acknowledgment. The corresponding author thanks to the projects DGAPA-PAPIIT: **TA101620**, **IT100321** and **IT102520**. Dulce Gonzalez-Utrera acknowledges to postdoctoral research grant from CONACyT México.

References

1. Rand, R., Applegate, R.A., Howland, H.C.: A mathematical model of Placido disk keratometer and its implication for recovery of corneal topography. In: Vision Science and Its Applications. OSA Technical Digest Series, 1, pp. 46–49, (1997)
2. Schwiegerling, J., Miller, J.M.: A videokeratoscope using a distorted checkerboard target. In: Vision Science and Its Applications (OSA Annual Meeting), (1998)
3. Klein, S.A.: Axial curvature and the skew ray error in corneal topography. In: Vision Science and Its Applications, 74, pp. 931–994, (1997)
4. Klein, S.A.: Corneal topography reconstruction algorithm that avoids the skew ray ambiguity and the skew error. In: Vision Science and Its Applications, 74, pp. 945–962, (1997)
5. Campos-García, M., Cossio-Guerrero, C., Moreno-Oliva, V.I., Huerta-Carranza, O.: Surface shape evaluation with a corneal topographer based on a conical null-screen with a novel radial point distribution. Applied Optics, 54, pp. 5411–5419, (2015)
6. Rodríguez-Rodríguez, M.I., Jaramillo-Nuñez, A., Díaz-Uribe, R.: Dynamic point shifting with null screen using three LCDs as targets for corneal topography. Applied Optics, 54, pp. 6698–6710, (2015)
7. Mejía-Barbosa, Y., Malacara-Hernández, D.: Object surface for applying a modified Hartmann test to measure corneal topography. Applied Optics, 40, pp. 5778–5786, (2001)
8. Díaz-Uribe, R., Campos-García, M.: Null-screen testing of fast convex aspheric surfaces. Applied Optics, 39, pp. 2670–2677, (2000)
9. Gonzalez Utrera, D., Aguirre-Aguirre, D., Rodríguez-Rodríguez, M.I., Díaz-Uribe, R.: Null-screen testing of the complementary freeform surfaces of an adjustable focus lens. Optics Express, 29(14), pp. 21698–21710, (2021)
10. Rodríguez-Rodríguez, M.I., Carmichael Martins, A., Vohnsen, B., Díaz-Uribe, R., Malacara-Hernández, D.: Corneal topographer using a Hartmann patterned. In: Proceedings of RIAO, (2019)
11. Aguirre-Aguirre, D., Díaz-Uribe, R., Campos-García, M., Villalobos-Mendoza, B., Izazaga-Pérez, R., Huerta-Carranza, O.: Fast conical surfaces evaluation with null-screen and randomized algorithms. Applied Optics, 56, pp. 1370–1382, (2017)

12. Díaz-Uribe, R.: Medium precision null screen testing of off-axis parabolic mirrors for segmented primary telescope optics; the case of the Large Millimetric Telescope. Applied Optics, 39, pp. 2790–2804, (2000)
13. Noll, R.J.: Zernike polynomials and atmospheric turbulence. Journal of the Optical Society of America, 66, pp. 207–211, (1976)

ISSN 1870-4069

Optical Switching by Thermocavitation for the Implementation of an All-Fiber Pulsed Laser

R. Zaca-Morán[1], P. Zaca-Morán[2], C. Amaxal-Cuatetl[2], J. Castillo-Mixcóatl[1], R. Ramos-García[3], J. P. Padilla-Martínez[2,*]

[1] Benemérita Universidad Autónoma de Puebla, FCFM, , Mexico

[2] Benemérita Universidad Autónoma de Puebla, Instituto de Ciencias, , Mexico

[3] Instituto Nacional de Astrofísica, Departamento de óptica, Óptica y Electrónica, Mexico

juan.padilla@correo.buap.mx

Abstract. A new optical switching for the generation of laser pulses based on the phenomenon of thermocavitation is reported. Thermocavitation bubbles were induced within a glass cuvette filled with a saturated solution of copper nitrate dissolved in water. Two optical fibers were submerged into the solution, very close to the region where the vapor bubble was generated. Once the bubble is generated it expands rapidly and the incoming laser light transmitted through the optical fiber is reflected at the vapor-solution interface and reflected into the fiber, which is coupled to an erbium-doped fiber ring laser and the laser pulse was extracted from the ring cavity and detected by a fast photodetector. The generation of the laser pulses is based on the change of the optical reflection coefficient at the end surface of the glass fiber by the expansion and collapse of the bubble, which behaves like a mirror with variable reflectivity. For both pulses, the repetition rate obtained was in a range of 118 Hz to 2 kHz at 1560 nm, with a pulse width ranging from 64 to 57 μs, which can be controlled by adjusting the laser power to in-duce thermocavitation bubbles.

Keywords: Optical switch, thermocavitation bubbles, pulsed laser.

1 Introduction

The basic scheme of a resonator for a fiber optic laser is the linear scheme, where the mirrors are deposited at the ends of the fiber [1]. But there are also resonators in ring configuration without mirrors, instead a coupler is used as the output port to extract the light emitted [2]. The modulation techniques for the generation of light pulses can be

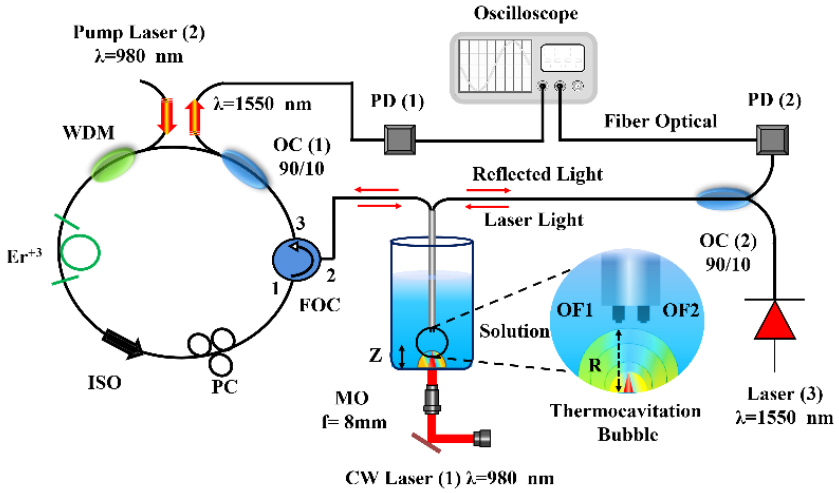

Fig. 1. Scheme of the thermocavitation-based pulsed laser and experimental setup known as a fiber optic hydrophone (FOH).

carried out in two different ways: i) Q-switching [2] and ii) Mode-Locking switching [3] which are divided in active and passive methods. In active methods the losses are modulated with elements external to the cavity with a control element [4] and passive methods, referring to internal elements that automatically modulate losses [5].

The phenomenon of thermocavitation is present when a highly absorbent solution is irradiated with a continuous wave (CW) laser. Where the absorbed light heats the solution to its critical limit, that is, the temperature at which an explosive liquid-gas phase transition occurs [6, 7]. The precise moment when superheated water explosively turns into steam, producing a rapidly expanding bubble, which finally collapses, emitting an acoustic wave. In this work, it is precisely the growth dynamics of the thermocavitation bubble the main factor that causes the losses and the control of the laser cavity, acting as a mirror of variable reflectivity in time.

2 Experimental setup

The thermocavitation is generated by a CW near infrared laser with λ = 980 nm (Laser (1)) where the output beam is collimated, reflected, and focused with a microscope objective (f = 8 mm) into the saturated solution of copper nitrate (13.78 g per 10 ml of water) which is contained inside a glass cuvette as shown in Fig. 1.

To carry out the generation of light pulses, the experimental setup of a pulsed all-fiber laser in a ring configuration with a total length of ~ 42 meters was used, see Fig. 1 (left section). The system was pumped by an LDC 205C laser with a wavelength λ = 980 nm (Laser 2), used 12 m of single-mode optical fiber doped with erbium as active medium, an WDM (NPM07000165), isolator (M11 / 81202003), polarization controller (FPC030) and an circulator (FOC) (S/N: A8038188), where the Port 1 of the FOC is

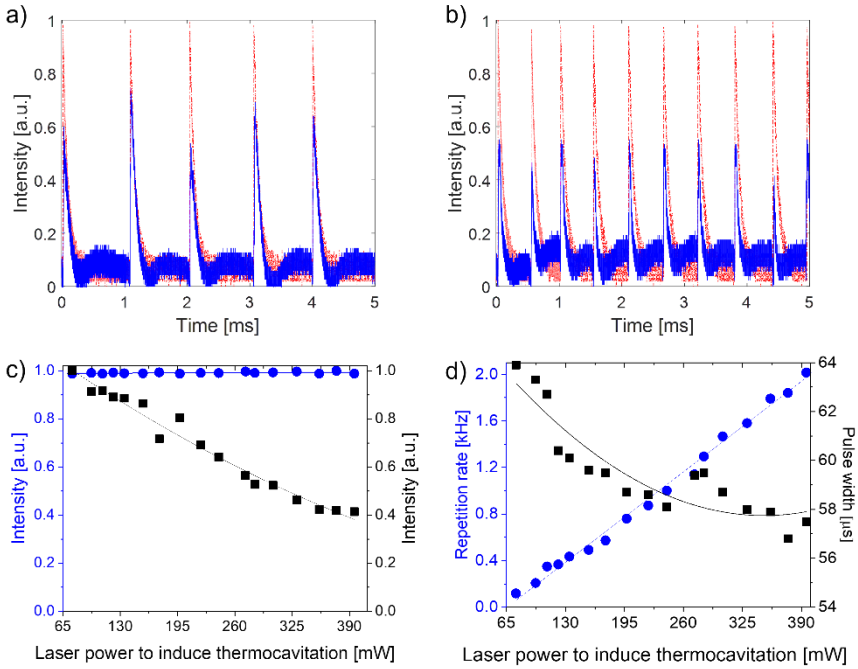

Fig. 2. Light pulses at the exit of the laser cavity (Red-Dotted) and the acoustic hydrophone (Blue-Continuous) varying the power to induce thermocavitation bubbles. a) 282 mW and b) 375 mW. c) Variation of intensities of the pulses extracted from the laser cavity (Blue-Circles) and those from the FOH (Black-Square), as well as in d) The repetition frequency (Blue-Circles) and the temporal width of the pulse (Square-Black) varying the power to induce thermocavitation.

connected to the laser cavity, while the optical fiber coming from port 2 was cleaned, cut, and introduced into a metal tube and subsequently, immersed in the working solution, close to the region where thermocavitation is created.

Consequently, the light reflected inside the fiber enters the circulator again through the same port 2 and exits through port 3, which is connected to a 90/10 optical coupler (CWD07014557) (OC (1)) to close the laser cavity, where only 10% of the energy is extracted in the form of pulses, which were analyzed with the help of a photodetector (PD (1)) and observed with an oscilloscope.

The right section of the experimental setup corresponds to the well-known fiber optic hydrophone (FOH) see Fig. 1 [8], which was implemented in this work in order to verify that each pulse at the output of the pulsed all-fiber laser corresponded to a single thermocavitation event.

The experimental setup uses an infrared laser with a wavelength of $\lambda = 1550$ nm (Laser 3), sending the light beam to a 90/10 coupler (CWD07014557) (OC (2)) where 90% of the light is sent to port one. Simultaneously both fibers (OF1 and OF2) detect the change in refractive index due to the glass-vapor interface caused by the growth of

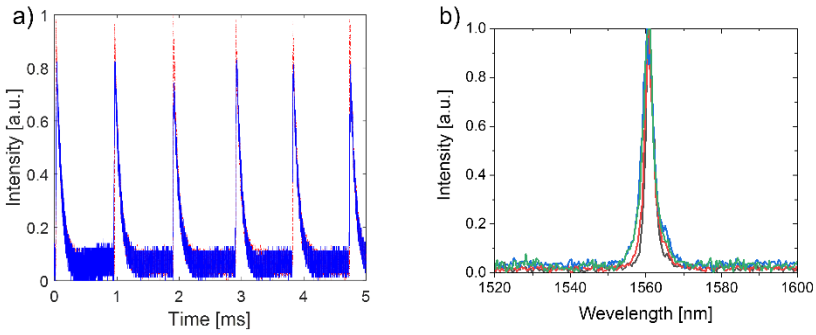

Fig. 3. a) Pulses at the output of the fiber optic laser (Red-Dotted) and the FOH (Blue-Continuous) at the pumping power of 272 mW. b) Spectra of the pulses at the exit of the cavity.

the thermocavitation bubble, which expands rapidly, causing the laser light to incoming transmitted through it is reflected.

3 Results

Figure 2 (a, b) shows the temporal characteristics of pulses, here the optic fiber laser (Red-Dotted) and the pulses detected by the fiber optic hydrophone (Blue-Continuous), were measured as a function of the laser power to induce thermocavitation (282 y 375 mW), using a power pump 235 mW to the laser ring. Both signals were observed simultaneously on the same oscilloscope, each pulse captured by the photodetector corresponds to a single thermocavitation event.

In the Fig. 2c shows the variation of normalized intensities captured by the oscilloscope of the pulses at the exit of the laser cavity (Blue-Circles), which remain practically constant. As well as the signals captured by FOH (Black-Boxes) which tend to decay, both signals detected as a function of the variation of the power to induce thermocavitation from 75 mW to 395 mW.

In Fig. 2d the repetition rate of the light pulses detected by the PD (1) that corresponds to the output of the laser cavity, which increases from 118 Hz to 2 kHz (Circles-Blue). while the temporal width decreases moderately from 64 to 57 μs (Squares-Black) both characteristics depending on the laser to induce thermocavitation.

To observe the variation of the temporal characteristics of the cavity output pulses when the pumping power is varied, the laser power to induce thermocavitation was set at 272 mW, as well the focusing distance $Z = 30$ μm.

Fig. 3a shows the temporary traces of the pulses at the exit of the cavity (Red-Dotted) and those detected by FOH (Blue-Continuous) at a pumping power of 199 mW, it was noted that the amplitude and the frequency is practically constant to the changes of variation in the bass drum power, so there is no need to show more sequences of pulses, the only alteration that the pulses present is in the temporal width with a decrease from 69 to 60.4 μs.

In Fig. 3b the output spectrum is shown, which is centered 1560 nm. More in detail about the pulses at the laser output, see the reference [9].

4 Conclusions

In this paper, we present a mechanism for the generation of laser pulses using the phenomenon of thermocavitation. Thermocavitation is due to the high laser light absorption by a homogeneous solution at a specific wavelength, which enables the focal point to reach superheated conditions (~300o C). Here, vapor bubbles were induced using a CW laser at 980 nm (which is an inexpensive energy source) focused into a saturable solution of copper nitrate dissolved in water.

Here the losses are caused by time-varying reflectivity due to the dynamic growth of a thermocavitation bubble. These reflectivity changes are detected by an optical fiber, which is coupled to a simple erbium-doped fiber ring laser. The amplitude of the laser pulses is greater and constant when they pass through the ring cavity, compared what the pulse is obtained from the fiber optic hydrophone setup.

Control over the pulse repetition rate is realized by adjusting the laser power to induce thermocavitation, obtaining a repetition rate from 118 Hz to 2 KHz, with a pulse width that change from 64 to 57 μs.

References

1. Yin, S., Ruffin, P.B., Francis, T.S.: Fiber Optic Sensors. CRC Press, (2017). doi: 10.1201/9781420053661.
2. Álvarez-Tamayo, R.I., Durán-Sánchez, M., Pottiez, O., Ibarra-Escamilla, B., Kuzin, E.A., Espinosa-Martínez, M.: Active Q-Switched Fiber Lasers with Single and Dual-Wavelength Operation. In: Fiber Laser, InTech, (2016)
3. Ennejah, T., Attia, R.: Mode Locked Fiber Lasers. In: Current Developments in Optical Fiber Technology, InTech, Chap 15, (2013). doi: 10.5772/46191.
4. Shen, Y., Wang, Y., Zhu, F., Ma, L., Zhao, L., Chen, Z., Feng, G.: 200 μJ, 13 ns Er: ZBLAN Mid-Infrared Fiber Laser Actively Q-Switched by an Electro-Optic Modulator. Optics Letters, 46(5), pp. 1141–1144, (2021). doi: 10.1364/OL.418950.
5. Zaca-Morán, P., Ortega-Mendoza, J.G., Lozano-Perera, G.J., Gómez-Pavón, L.C., Pérez-Sánchez, G.F., Padilla-Martínez, J.P., Felipe, C.: Passively Q-Switched Erbium-Doped Fiber Laser Based on Zn Nanoparticles as a Saturable Absorber. Laser Physics, 27(10), pp. 105101, (2017). doi: 10.1088/1555-6611/aa83e0.
6. Ramirez-San Juan, J.C., Rodriguez-Aboytes, E., Martinez-Canton, A.E., Baldovino-Pantaleon, O., Robledo-Martinez, A., Korneev, N., Ramos-Garcia, R.: Time-Resolved Analysis of Cavitation Induced by CW Lasers in Absorbing Liquids. Opt. Express, 18(9), pp. 8735–8742, (2010). doi: 10.1364/OE.18.008735.
7. Padilla-Martinez, J.P., Berrospe-Rodriguez, C., Aguilar, G., Ramirez-San-Juan, J.C., Ramos-Garcia, R.: Optic Cavitation with CW Lasers: A Review. Phys. Fluids, 26(12), pp. 122007, (2014). doi: 10.1063/1.4904718.
8. Arvengas, A., Davitt, K., Caupin, F.: Fiber Optic Probe Hydrophone for the Study of Acoustic Cavitation in Water. Rev. Sci. Instrum., 82(3), pp. 034904, (2011). doi: 10.1063/1.3557420.

9. Zaca-Morán, R., Amaxal-Cuatetl, C., Zaca-Morán, P., Castillo-Mixcóatl, J., Ramos-García, R., Padilla-Martínez, J.P.: Thermocavitation: A Mechanism to Pulse Fiber Lasers. Optics Express, 29(15), pp. 23439–23446, (2021). doi: 10.1364/OE.430319.

Electronic edition
Available online: http://www.rcs.cic.ipn.mx

http://rcs.cic.ipn.mx

Centro de Investigación
en Computación